

## WAVE PROPAGATION AT OBLIQUE SHOCKS: HOW DID TYCHO GET ITS STRIPES?

J. MARTIN LAMING<sup>1</sup>*Draft*

## ABSTRACT

We describe a new model for the “stripes” of synchrotron radiation seen in the remnant of Tycho’s supernova. In our picture, cosmic rays streaming ahead of the forward shock generate parallel propagating (with respect to the local magnetic field direction) circularly polarized Alfvén waves that are almost free of dissipation, and due to being circularly polarized exhibit no spatial variation of magnetic field strength. Following interaction with the SNR shock with nonzero obliquity, these parallel propagating waves become obliquely propagating, due to the wave refraction (different in principle for the different plane wave components), and dissipation sets in. The magnetosonic polarization decays faster, due to transit time damping, leaving only the Alfvén mode. This surviving mode now exhibits a spatial variation of the magnetic field, leading to local maxima and minima in the synchrotron emission, i.e. the stripes. We attribute the initial wave generation to the Bell instability, which in contrast to the resonant generation of upstream Alfvén waves, gives rise to a preferred wavelength, and hence the single wave period at which the stripes are seen. Based on estimates for damping rates due to turbulent cascade and transit time damping, we estimate the dependence of the visibility of the stripes on the shock obliquity, and determine a maximum cosmic ray energy in Tycho’s SNR in the range  $6 \times 10^{14} - 1 \times 10^{15}$  eV.

*Subject headings:* acceleration of particles — cosmic rays — magnetic fields — shock waves — ISM: supernova remnants

## 1. INTRODUCTION

The advent of the Chandra and XMM-Newton X-ray astronomy missions has revitalized the field of cosmic ray acceleration. Chandra’s combination of arcsecond resolution imaging and the moderate energy spectral resolution afforded by CCD X-ray detectors has proven well suited to the study of supernova remnants, and specifically the X-ray synchrotron radiation emitted by cosmic ray electrons. This often reveals itself as thin rims of continuum emission in the 4 - 6 keV waveband (a region essentially free of quasi-thermal line emission from shocked plasma) spatially coinciding with the supernova remnant forward shock. This can be understood (e.g. Vink & Laming 2003) as cosmic ray electrons radiating in the strong (i.e. amplified) magnetic field at the shock. The radial extent is limited by either the radiative loss time of the electrons, or the decay of magnetic field post-shock. The remnant of Tycho’s supernova shows an even more intriguing pattern of synchrotron radiation; a series of “stripes” or ripples, (Eriksen et al. 2011), observed most clearly in the 4 - 6 keV waveband where line emission from the quasi-thermal plasma in the SNR is absent. The wavelength corresponds to the gyroradius of cosmic ray protons with energies in the range  $10^{14} - 10^{15}$  eV, but the precise mechanism by which these structures form is not known.

The Bell instability (Bell 2004, 2005), which amplifies magnetic field in the shock precursor region, generates linearly polarized structures in a near perpendicular shock geometry. Considering the effect of these short wavelength fluctuations on the cosmic ray current, Vladimirov et al. (2009) and Bykov et al. (2011a)

have shown that long wavelength upstream structures can result, with spatial variations of the magnetic field strength and hence synchrotron emissivity. Bykov et al. (2011b) argue that these long wavelength structures are responsible for the “stripes”. A number of conditions must be met. Most importantly, the shock region where the stripes appear must be “nearly perpendicular” (Bykov et al. 2011b, don’t specify how close to 90° they require), and that in this nearly perpendicular region, shock acceleration must still be efficient. But as discussed elsewhere (Zank et al. 2006; Laming et al. 2013), the efficiency of shock acceleration at quasi-perpendicular shocks is open to question.

Malkov et al. (2012) offer an alternative idea, that is appears most promising at parallel shocks. They find fully nonlinear exact ideal MHD solutions supported by the cosmic ray return current, which comprise pulses of Alfvén waves that can propagate ahead of the main shock. Malkov et al. (2012) argue that these Alfvén pulses when visible in X-rays should appear as quasi-periodic stripes, with spacing similar to that of the observed stripes. In their equations, Malkov et al. (2012) neglect thermal and cosmic ray pressure gradients, assuming that the ponderomotive force of the turbulence is much stronger. In the opposite limit high frequency sound waves are generated by the Drury instability (Drury & Falle 1986). Caprioli & Spitkovsky (2013) suggest that the forward shock may push forwards in upstream cavities created at the saturation of the Bell instability, also at parallel shocks. Rakowski et al. (2011) discuss a similar idea in connection with shock structures (although not stripes) seen in SN 1006.

In this paper we pursue a different model for these synchrotron stripes in Tycho’s SNR. Cosmic rays drifting ahead of a quasi-parallel shock generate upstream

<sup>1</sup> Space Science Division, Naval Research Laboratory, Code 7684, Washington DC 20375 [laming@nrl.navy.mil](mailto:laming@nrl.navy.mil)

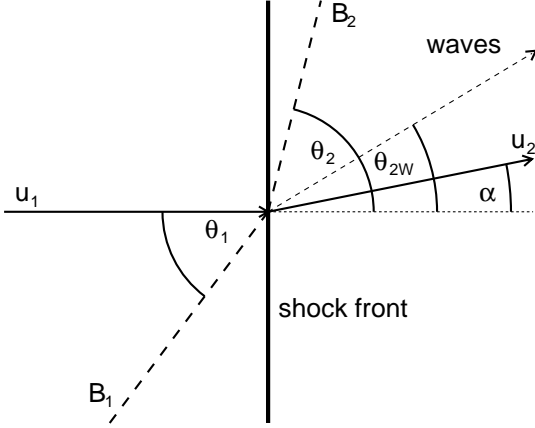


FIG. 1.— Schematic diagram of wave propagation at the oblique shock, in the shock rest frame. Upstream (left), plasma moves towards the shock front with velocity  $\mathbf{u}_1$ , carrying with it magnetic field  $\mathbf{B}_1$  at angle  $\theta_1$  to  $\mathbf{u}_1$  (or the shock normal). Postshock, the magnetic field is  $\mathbf{B}_2$  at angle  $\theta_2$  to the shock normal and the flow velocity is  $\mathbf{u}_2$  at angle  $\alpha$  to the shock normal. In the preshock medium, waves are assumed to be parallel propagating along  $\mathbf{B}_1$ . Postshock, the waves refract and travel at an angle  $\theta_{2W}$  to the shock normal. They are no longer parallel propagating. In principle, Alfvén and magnetosonic polarizations will refract at slightly different angles. The difference between these two angles of refraction tends to zero as the Alfvén Mach number  $M_A \rightarrow \infty$ , the approximation taken in this paper.

circularly polarized Alfvén waves. We assume these to be parallel propagating (see e.g. Bamert et al. 2004; Gargaté & Spitkovsky 2012), and with no spatial variation in magnetic field pressure. Upon passage through the shock, both the magnetic field and the wave propagation change direction, and by different amounts, so that the formerly parallel propagating waves are now obliquely propagating. The circular polarization decomposes into its linearly polarized constituents. The magnetosonic polarization becomes compressive, and quickly decays by transit time damping. The Alfvén polarization survives longer, and its spatially varying magnetic field gives rise the regions of enhanced synchrotron emission, observable as the stripes or ripples seen by Eriksen et al. (2011). The following sections treat the wave refraction at the shock, the wave transmission and reflection coefficients, and the postshock damping of the magnetosonic and Alfvén modes. Section 5 puts these topics together to explain the origin of the stripes, and to derive physical implications from this identification.

## 2. WAVE REFRACTION AT SHOCKS

McKenzie & Westphal (1970) and Webb et al. (1999) give formal accounts of wave properties at oblique shocks. We follow and extend slightly for our particular application the more pedagogical treatment of Achterberg & Blandford (1986). A schematic diagram of the wave propagation at an oblique shock is shown in Fig 1. In the preshock medium, we take both Alfvén and magnetosonic polarizations to be parallel propagating (with respect to the upstream magnetic field) with phase velocity  $V_{A1}$ , the upstream Alfvén speed. Downstream, the Alfvén polarization has phase speed  $V_{A2} \cos(\theta_2 - \theta_{2W})$ , where  $\theta_2$  is the angle from the shock normal to the postshock magnetic field, and  $\theta_{2W}$  is the angle from the shock normal to the wave propagation direction. The phase speed of the magnetosonic wave depends on the plasma beta (the ratio of gas pressure to

magnetic pressure), and is given by (e.g Melrose 1986)

$$v^2 = \frac{1}{2} \left( V_{A2}^2 + c_{s2}^2 \pm \left[ (V_{A2}^2 + c_{s2}^2)^2 - 4V_{A2}^2 c_{s2}^2 \cos^2(\theta_2 - \theta_{2W}) \right]^{1/2} \right) \\ \simeq V_{A2}^2 \cos^2(\theta_2 - \theta_{2W}) - \frac{V_{A2}^4}{c_{s2}^2} [\cos^2(\theta_2 - \theta_{2W}) + \cos^4(\theta_2 - \theta_{2W})] + \dots \quad \beta \gg 1 \quad (1) \\ \simeq V_{A2}^2 + c_{s2}^2 \sin^2(\theta_2 - \theta_{2W}) \quad \beta < 1. \quad (2)$$

In the following we will only consider the leading terms in equations 1 and 2, which will lead to the same angle of refraction  $\theta_{2W}$  for both polarizations. In principle, however, the different polarizations can refract at slightly different angles. At the shock transition, we demand that the phases of upstream and downstream waves are equal, i.e.  $\omega_1 t - \mathbf{k}_1 \cdot \mathbf{r} = \omega_2 t - \mathbf{k}_2 \cdot \mathbf{r}$ , and that the components of wavevectors perpendicular to the shock velocity are continuous. For magnetosonic waves at low  $\beta$  these constraints give the equations

$$k_1 V_{A1} - k_1 \cos \theta_1 u_1 = k_2 V_{A2} - k_2 u_2 \cos(\theta_{2W} - \alpha) \quad (3)$$

$$k_1 \sin \theta_1 = k_2 \sin \theta_{2W}, \quad (4)$$

where  $\tan \alpha = u_{2\perp}/u_{2\parallel} = ru_{2\perp}/u_{1\parallel}$ , the tangent of the angle the postshock flow makes to the shock normal with  $r$  being the shock compression ratio. Dividing (3) by (4) to eliminate  $k_1$  and  $k_2$  leads to

$$\frac{V_{A1}}{\sin \theta_1} - u_1 \cot \theta_1 = \frac{V_{A2}}{\sin \theta_{2W}} - u_2 \cot \theta_{2W} \cos \alpha - u_2 \sin \alpha, \quad (5)$$

which can be rearranged to give an equation for  $\theta_{2W}$ ;

$$\frac{M_{A2} \cos \theta_{2W} - 1}{M_{A2} \sin \theta_{2W}} = r \frac{M_{A1} \cos \theta_1 - 1}{M_{A1} \sin \theta_1} - \tan \alpha. \quad (6)$$

For  $M_{A1} \rightarrow \infty$ ,  $M_{A2} \rightarrow \infty$ , (and hence  $\tan \alpha \rightarrow 0$ ) and well away from the precisely perpendicular shock where  $\cos \theta_{2W} = \cos \theta_1 = 0$ , this reduces to

$$\cot \theta_{2W} = r \cot \theta_1 = \frac{r^2}{\tan \theta_2} \quad (7)$$

where we have also used the result  $\tan \theta_2 = r \tan \theta_1$  from equation A4. Writing  $\tan \theta_{2W} = \tan(\theta_2 - \Delta)$  where  $\Delta$  is the angle between the magnetosonic wave propagation direction and the postshock magnetic field direction, we find

$$\tan \Delta = \frac{(r^2 - 1)}{r} \cos \theta_1 \sin \theta_1. \quad (8)$$

The maximum deviation of the wave propagation from the magnetic field, and hence the maximum wave compression is achieved for  $\theta_1 = 45^\circ$ , where  $\tan \Delta = -15/8$  (assuming  $r = 4$ ) and  $\Delta = 62^\circ$ . Solving for  $\theta_2$  we find  $\theta_2 = 76^\circ$  and  $\theta_{2W} = 14^\circ$ .

For magnetosonic waves at high  $\beta$  and for Alfvén waves equation 3 above becomes

$$k_1 V_{A1} - k_1 \cos \theta_1 u_1 = k_2 V_{A2} \cos(\theta_{2W} - \theta_2) - k_2 u_2 \cos(\theta_{2W} - \alpha) \quad (9)$$

accounting for the different dispersion properties of the Alfvén wave. Following the same approach as above, we find

$$\frac{M_{A2} - \cos \theta_2}{M_{A2}} \cot \theta_{2W} = r \cot \theta_1 - \frac{r}{M_{A1} \sin \theta_1} - \tan \alpha + \frac{\sin \theta_2}{M_{A2}}, \quad (10)$$

which can be recast as

$$\left(1 - \frac{r^{1/2} \cos \theta_1}{M_{A1}}\right) \cot \theta_{2W} = r \cot \theta_1 - \frac{r}{M_{A1} \sin \theta_1} - \tan \alpha + \frac{r^{3/2} \sin \theta_1}{M_{A1}}. \quad (11)$$

In the limit  $M_{A1} \rightarrow \infty$ , ensuring  $\beta \gg 1$  in the postshock medium, this reduces to  $\cot \theta_{2W} = r \cot \theta_1$  as above. Away from this limit,  $\cot \theta_{2W}$  will be different for magnetosonic and Alfvén modes. In supernova remnants, this is unlikely to be a significant effect, but in the lower  $M_{A1}$  shocks driven by solar coronal mass ejections, this could be an important consideration. The limit  $M_{A1} \rightarrow \infty$  also captures the case when  $\omega_1 \rightarrow 0$ , appropriate for the Bell nonresonant instability where modes grow at zero frequency.

### 3. WAVE TRANSMISSION AND REFLECTION AT SHOCKS

Vainio & Schlickeiser (1999) give transmission and reflection coefficients for forward and backward propagating Alfvén waves at a parallel shock. Using the jump conditions for the tangential electric field,

$$[u_n B_t - B_n u_t] = 0, \quad (12)$$

the continuity of the transverse momentum,

$$[\rho u_n u_t - B_n B_t / 4\pi] = 0, \quad (13)$$

and the continuity of the mass flux

$$[\rho u_n] = 0, \quad (14)$$

their result is

$$\frac{T}{R} = \frac{(M_{A1} + H)(\sqrt{r} \pm 1)\sqrt{r}}{2(M_{A1} \pm H\sqrt{r})}. \quad (15)$$

Here  $M_A$  is the Alfvén Mach number of the shock, and  $H$  is the cross helicity of the waves.  $H = 1$  for forward and  $H = -1$  for backward propagating waves. At a parallel shock, the two polarizations, Alfvén and magnetosonic, behave the same. At an oblique shock, differences emerge. For the Alfvén mode, which perturbs magnetic field and velocity in the direction perpendicular to the plane in which the wave refraction occurs, results for  $T$  and  $R$  are obtained from equation 15 with the replacement  $M_{A1} \rightarrow M_{A1} / \cos \theta_1$ .

The magnetosonic mode is much more involved since perturbed magnetic field and velocity vectors lie in the plane of refraction. It appears to be tractable only in the limit  $M_{A1} \rightarrow \infty$ , when the motion of the shock front itself in response to the passing wave can be neglected. We evaluate the jump conditions for the tangential electric field and the continuity of transverse momentum using

$$B_n = -B_2 \cos \theta_2 + \delta B \sin \theta_{2W} \quad (16)$$

$$B_t = B_2 \sin \theta_2 + \delta B \cos \theta_{2W} \quad (17)$$

$$u_n = -u_{2\parallel} + \delta u \sin \theta_{2W} \quad (18)$$

$$u_t = u_{2\perp} + \delta u \cos \theta_{2W}. \quad (19)$$

Substituting into the first jump condition gives

$$\begin{aligned} & \left(-u_1 + \delta u_1^f \sin \theta_1\right) \left(B_1 \sin \theta_1 + \delta B_1^f \cos \theta_1\right) \\ & - \left(-B_1 \cos \theta_1 + \delta B_1^f \sin \theta_1\right) \delta u_1^f \cos \theta_1 \\ & = \left(-u_{2\parallel} + \delta u_2 \sin \theta_{2W}\right) \left(B_2 \sin \theta_2 + \delta B_s \cos \theta_{2W}\right) \\ & - \left(-B_2 \cos \theta_2 + \delta B_s \sin \theta_{2W}\right) \left(u_{2\perp} + \delta u_s \cos \theta_{2W}\right). \end{aligned} \quad (20)$$

Multiplying out and assuming  $-u_1 B_1 \sin \theta_1 = -u_{2\parallel} B_2 \sin \theta_2 - u_{2\perp} B_2 \cos \theta_2$  yields

$$\begin{aligned} & \delta u_1 B_1 - u_1 \delta B_1 \cos \theta_1 = \delta u_2 B_2 \cos (\theta_2 - \theta_{2W}) \\ & - u_{2\parallel} \delta B_2 \cos \theta_{2W} - u_{2\perp} \delta B_2 \sin \theta_{2W}. \end{aligned} \quad (21)$$

We put  $\delta u_1 = \delta u_1^f$  or  $\delta u_1^b$  to represent an initially forward or backward propagating wave, and then put  $\delta u_2 = \delta u_2^f + \delta u_2^b = (-\delta B_2^f + \delta B_2^b) / \sqrt{4\pi\rho_2}$  and rearrange to find

$$\begin{aligned} M_{A1} \cos \theta_1 \pm 1 = & \frac{T^f}{R^b} \left\{ \frac{B_2}{\sqrt{r} B_1} \cos (\theta_2 - \theta_{2W}) \right. \\ & + \frac{M_{A1}}{r} \cos \theta_{2W} + M_{A1} \frac{u_{2\perp}}{u_1} \sin \theta_{2W} \left. \right\} \\ & - \frac{R^f}{T^b} \left\{ \frac{B_2}{\sqrt{r} B_1} \cos (\theta_2 - \theta_{2W}) - \frac{M_{A1}}{r} \cos \theta_{2W} \right. \\ & \left. - M_{A1} \frac{u_{2\perp}}{u_1} \sin \theta_{2W} \right\}. \end{aligned} \quad (22)$$

The +ve sign in the left hand side corresponds to  $T_f = \delta B_2^f / \delta B_1^f$  and  $R^f = \delta B_2^b / \delta B_1^f$ , while the -ve sign corresponds to  $R^b = \delta B_2^f / \delta B_1^b$  and  $T^b = \delta B_2^b / \delta B_1^b$ . A similar procedure for the second jump condition gives

$$\begin{aligned} \pm M_{A1} \cos \theta_1 + \cos 2\theta_1 = & \frac{T^f}{R^b} \left\{ \frac{M_{A1}}{\sqrt{r}} \cos \theta_{2W} \right. \\ & - M_{A1} \sqrt{r} \frac{u_{2\perp}}{u_1} \sin \theta_{2W} + \frac{B_2}{B_1} \cos (\theta_2 + \theta_{2W}) \left. \right\} \\ & + \frac{R^f}{T^b} \left\{ -\frac{M_{A1}}{\sqrt{r}} \cos \theta_{2W} + M_{A1} \sqrt{r} \frac{u_{2\perp}}{u_1} \sin \theta_{2W} \right. \\ & \left. + \frac{B_2}{B_1} \cos (\theta_2 + \theta_{2W}) \right\}. \end{aligned} \quad (23)$$

Taking  $M_{A1} \rightarrow \infty$ , so that also  $u_{2\perp} \rightarrow 0$  in equations 22 and 23 we find

$$\begin{aligned} \frac{T^{bf}}{R^{bf}} = & \frac{\cos \theta_1}{2 \cos \theta_{2W}} \sqrt{r} (\sqrt{r} \pm 1) \\ = & \left( \frac{\sqrt{r} \pm 1}{2\sqrt{r}} \right) \sqrt{\sin^2 \theta_1 + r^2 \cos^2 \theta_1}, \end{aligned} \quad (24)$$

where we have substituted from  $\cot \theta_{2W} = r \cot \theta_1$  in the final step. This agrees with Vainio & Schlickeiser (1999) and equation 15 in the appropriate limits ( $\theta_1 \rightarrow 0$  and  $M_{A1} \rightarrow \infty$ ).

The forgoing has treated Alfvén and magnetosonic waves of nonzero frequency in the upstream and downstream shock regions. As mentioned above, when being driven by the cosmic ray current, these waves grow in the upstream region at zero frequency, and hence  $\delta u_1 \Rightarrow 0$ . In equations 22 and 23 this leads to the terms  $\pm 1$  and  $\pm M_{A1} \cos \theta_1$  on the left hand sides of equation 22 and 23 respectively being dropped. We give the corresponding expression for the transmission and reflection coefficients for Alfvén (A) and magnetosonic (M) modes

$$\begin{aligned} T &= \frac{M_{A1} r / \cos \theta_1 \pm H \sqrt{r}}{2 (M_{A1} / \cos \theta_1 \pm H \sqrt{r})} \rightarrow \frac{r}{2} \quad (\text{A}) \\ R &= \frac{1}{2} \sqrt{\sin^2 \theta_1 + r^2 \cos^2 \theta_1} \quad (\text{M}), \end{aligned} \quad (25)$$

which are independent of the cross-helicity  $H$  in the limit that  $M_{A1} \rightarrow \infty$ .

#### 4. WAVE DAMPING

Behind the shock, the newly obliquely propagating waves are subject to various damping mechanisms. Both Alfvén and magnetosonic polarizations decay by turbulent cascade, and the magnetosonic wave, now compressive due to its oblique propagation also decays by transit time damping by the shocked quasi-thermal ions.

Many formulations exist for the damping by turbulent cascade. We follow Boldyrev (2005) who gives an expression to cover the cases of both the weak turbulence (Goldreich & Sridhar 1995) and strong turbulence (Iroshnikov 1963; Kraichnan 1965). In these limits the approximate damping rates for the large scale turbulence are

$$\gamma_{GS} = k_{2\parallel} \delta u_2 = \omega \tan(\theta_2 - \theta_{2W}) \delta u_2 / V_{A2} \quad (26)$$

$$\gamma_{IK} = k_{2\perp} \delta u_2^2 / V_{A2} = \omega \tan(\theta_2 - \theta_{2W}) \delta u_2^2 / V_{A2}^2, \quad (27)$$

where  $\omega = k_{2\parallel} V_{A2}$  from equation 1. The strong turbulence expression for  $\gamma_{IK}$  is probably the most applicable. These simplest expressions refer to balanced turbulence, with equal wave amplitudes propagating in each direction. In our case, and decay rate of the transmitted waves will depend on the intensity of counter propagating reflected waves, and vice versa. We will assume cosmic rays streaming ahead of the shock generate wave travelling in one direction only (away from the shock), and then we will take  $\delta u_2 = \delta u_1 R$ , where  $R$  is the reflection coefficient calculated above in equation 24, in the damping rates.

The magnetosonic polarization is also subject to transit time damping by shocked but quasi-thermal ions. This damping rate in the small gyroradius limit is given by (Melrose 1986)

$$\begin{aligned} \gamma_{TTD} &= - \int \int \frac{4\pi^2 q^2 V_{A2}^2}{\hbar \omega c^2} \left( \frac{v_{\perp}^2 k_{\perp}}{\Omega} \right)^2 \delta(\omega - k_{\parallel} v_{\parallel}) \\ &\times \hbar k_{\parallel} \frac{\partial f}{\partial p_{\parallel}} 2\pi p_{\perp} dp_{\perp} dp_{\parallel}, \end{aligned} \quad (28)$$

where  $\omega$  and  $\Omega$  are the wave angular frequency and thermal ion gyrofrequency respectively,  $V_{A2}$  is the postshock Alfvén speed, and  $v$  and  $p$  are the ion velocity and momentum respectively, with subscripts  $\perp$  and  $\parallel$  indicating components perpendicular or parallel to the ambient

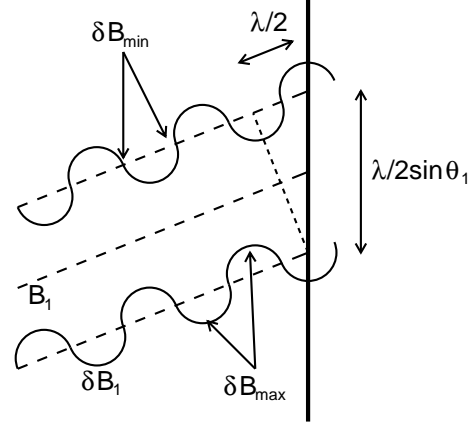


FIG. 2.— Schematic diagram of a plane parallel wave front encountering the shock. Upstream the wave is a parallel propagating circularly polarized wave, with no spatial variation in the magnetic field strength. Behind the shock the magnetosonic polarization is damped quickly, leaving a spatial variation in magnetic field strength due to the surviving Alfvén polarization, with maxima every half wavelength along the wave propagation direction,  $\lambda_1/2$ , as indicated. When projected onto the shock front the distance between magnetic field maxima becomes  $\lambda_1/2 \sin \theta_1$ , where  $\theta_1$  is the shock obliquity, the angle of the upstream unperturbed magnetic field to the shock normal.

magnetic field. We represent the ion distribution function  $f$  as a “kappa” distribution;

$$f = \frac{n}{(2\pi)^{3/2} m^3 v_{Th2}^3} \frac{\Gamma(\kappa)}{\Gamma(\kappa - 3/2) \kappa^{3/2}} \left[ 1 + \frac{p^2}{2\kappa^2 v_{Th2}^2} \right]^{-\kappa}, \quad (29)$$

where  $m$  is the ion mass,  $v_{Th2}$  is its thermal velocity,  $\Gamma(\kappa)$  is the Gamma function of with argument  $\kappa$ , and  $\kappa$  is the index of the distribution. For  $\kappa \rightarrow \infty$ ,  $f$  tends to a Maxwellian. For finite  $\kappa$ , the kappa distribution has extended wings compared to a Maxwellian, and may be taken to represent suprathermal ions in addition to the Maxwellian core. Normalizing the kappa distribution over an infinite momentum range, we require  $\kappa > 3/2$  to keep the number density  $n$  finite, and  $\kappa > 5/2$  to keep the energy finite. Smaller values of kappa require a high-momentum cutoff to keep particle number and energy densities finite. Substituting equation 29 into equation 28 we get

$$\begin{aligned} \gamma_{TTD} &= \frac{2\pi^2 q^2 V_{A2}^2}{m^7 v_{Th2}^5 \Omega^2 c^2} \frac{k_{\perp}^2}{k_{\parallel}} \sqrt{\frac{2}{\pi}} \frac{n \Gamma(\kappa)}{\Gamma(\kappa - 3/2) \kappa^{3/2}} \\ &\times (2\kappa m^2 v_{Th2}^2)^{\kappa+1} \\ &\times \int_0^\infty \left[ 2\kappa m^2 v_{Th2}^2 + \frac{m^2 \omega^2}{k_{\parallel}^2} + p_{\perp}^2 \right]^{-\kappa-1} p_{\perp}^5 dp_{\perp}. \end{aligned} \quad (30)$$

The integral is performed by substituting  $p_{\perp} = \sqrt{m^2 \omega^2 / k_{\parallel}^2 + 2\kappa m^2 v_{Th2}^2} \tan \psi$  and evaluating the resulting integral,  $\int_0^{\pi/2} \sin^5 \psi \cos^{2\kappa-5} \psi d\psi = \int_0^1 (1 - \cos^2 \psi)^2 \cos^{2\kappa-5} \psi d(\cos \psi)$  to find

$$\begin{aligned} \gamma_{TTD} &= \frac{2\pi^2 q^2 n V_{A2}^2}{m \Omega^2 c^2} \frac{k_{\perp}^2 v_{Th2}}{k_{\parallel}} \sqrt{\frac{2}{\pi}} \left[ 1 + \frac{V_{A2}^2}{2\kappa v_{Th2}^2} \right]^{2-\kappa} \\ &\times \frac{\Gamma(\kappa)}{\Gamma(\kappa - 3/2) \kappa^{3/2}} \frac{8\kappa^2}{(\kappa - 1)(\kappa - 2)}. \end{aligned} \quad (31)$$

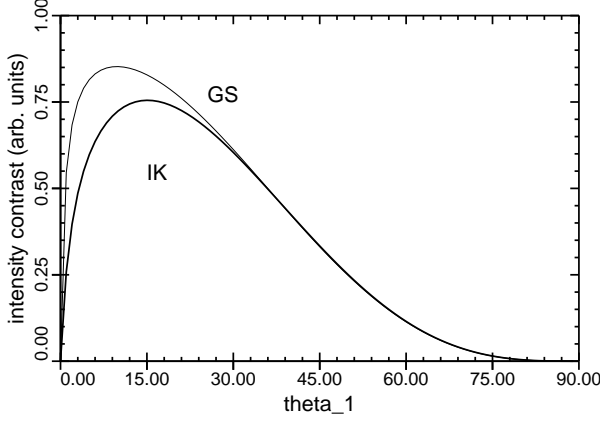


FIG. 3.— Variation with shock obliquity  $\theta_{BN}$  of the intensity contrast  $\Delta I$  between stripe maxima and minima, for the cases of Iroshnikov-Kraichnan (IK) or Goldreich-Sridhar (GS) turbulence.

As  $\kappa \rightarrow \infty$ ,  $\gamma_{TTD} \rightarrow 4\sqrt{2\pi}k_{\perp}^2 v_{Th2} \exp(-1/\beta)/k_{\parallel}$ . For application below, where  $\beta \gg 1$  and  $\omega \simeq k_{\parallel}V_{A2}$ , we rewrite as

$$\gamma_{TTD} \simeq 4\sqrt{2\pi}\omega \tan^2(\theta_2 - \theta_{2W}) v_{Th2}/V_{A2}. \quad (32)$$

For a fast shock neglecting energy losses to cosmic rays,  $v_{Th2} \simeq \sqrt{3}v_s/4 \sim 2000 \text{ km s}^{-1}$ , where the shock velocity in Tycho  $v_s \simeq 5000 \text{ km s}^{-1}$ .

## 5. HOW DID TYCHO GET ITS STRIPES?

Eriksen et al. (2011) observe “stripes” in synchrotron emission from Tycho’s SNR. The stripes are separated by about  $10''$ , which corresponds to  $6 \times 10^{17} \text{ cm}$  at the presumed 4.0 kpc distance (Hayato et al. 2010), or  $5 \times 10^{17} \text{ cm}$  at 3.2 kpc (Slane et al. 2014). We argue that these structures arise at oblique shocks, where upstream parallel circularly polarized waves which are undamped become obliquely propagating damped waves postshock. The key point is that the magnetosonic polarization damps faster than the Alfvén polarization, and so a spatial variation in the magnetic field strength will emerge associated with the surviving Alfvén mode. Along the direction of propagation the absolute magnitude of the magnetic field strength has a maximum every half wavelength ( $\lambda_1/2$ ). When projected onto the shock front, the maxima are separated by a distance of  $\lambda_1/2 \sin \theta_1$ , as shown schematically in Fig 2. Although less damped than the magnetosonic polarization, the Alfvén modes still damp within a wavelength or so postshock. These magnetic field variations are illuminated by synchrotron radiation from cosmic ray electrons, the radiative cooling time for which typically lies between the magnetosonic and Alfvén mode damping times. This hierarchy ensures that the damped magnetosonic polarization does not contribute significantly to the emission, while the Alfvén mode only contributes close to the shock, while the electrons are still radiating in X-rays.

In the case of Iroshnikov-Kraichnan turbulence, the difference in synchrotron intensity between maxima and minima in the stripes may be written

$$\Delta I \propto \left[ \exp(-\gamma_{IK}t)^{s+1} - \exp(-\gamma_{IK}t - \gamma_{TTD}t)^{s+1} \right] \times \cos^{s+1} \theta_1 \quad (33)$$

where  $s$  is the index of the synchrotron photon spec-

trum and  $s+1$  is the power law dependence of the magnetic field strength on the synchrotron emission. The final factor of  $\cos \theta_1$  gives the approximate shock obliquity dependence of the preshock magnetic field amplification. Goldreich-Sridhar turbulence simply requires  $\gamma_{GS}$  in place of  $\gamma_{IK}$ . This intensity contrast is maximized at  $t = \ln(1 + \gamma_{TTD}/\gamma_{IK})/\gamma_{TTD}/(s+1)$  with value

$$\Delta I \propto \left[ \exp(-\gamma_{IK}/\gamma_{TTD}) \ln(1 + \gamma_{TTD}/\gamma_{IK}) - \exp(-\gamma_{IK}/\gamma_{TTD} - 1) \ln(1 + \gamma_{TTD}/\gamma_{IK}) \right] \times \cos^{s+1} \theta_1. \quad (34)$$

Figure 3 shows the dependence of  $\Delta I$  on the shock obliquity  $\theta_1$ , for both Iroshnikov-Kraichnan (IK; strong) turbulence and Goldreich-Sridhar (GS; weak) turbulence, calculated from equation 34, using equations 26, 27, and 32. We take  $\delta u_2 = \delta u_1 R$ , and  $\delta u_1 \simeq 180 \text{ km s}^{-1}$ , corresponding to  $R \simeq 2$  from equations 25, and postshock magnetic field and density of  $180 \mu\text{G}$  and  $1.2 \text{ amu cm}^{-3}$  respectively (Slane et al. 2014). In both cases the emission is relatively strongly peaked over a restricted range of angles, possibly suggesting a reason why the stripes are not ubiquitous over Tycho, but only seen in certain “special” regions.

The separation at which the stripes preferably appear can be used to estimate the maximum cosmic ray ion energy in Tycho. The Bell instability grows structures at a parallel wavevector in the ambient magnetic field given by (Bell 2004, 2005; Laming et al. 2014)

$$k_{\parallel} = 1.5 \times 10^{-8} \eta n_i \left( \frac{u_1}{5000 \text{ km s}^{-1}} \right)^3 \left( \frac{3\mu \text{ G}}{B} \right) \times \frac{\gamma_{max} - 3\gamma_1/4}{\gamma_{max}\gamma_1 (\ln \gamma_{max} - 1)} = \frac{2\pi}{\lambda_1}. \quad (35)$$

Here  $\eta$  is the fraction of shock energy going into cosmic rays,  $n_i$  is the ion number density in the preshock medium. The highest energy cosmic rays have Lorentz factor  $\gamma_{max}$ , while the highest energy magnetized cosmic rays have Lorentz factor  $\gamma_1$ . The cosmic ray current with particles with  $\gamma_1 < \gamma < \gamma_{max}$  drives the Bell instability. We have also set  $\delta B/B = 1$  in equation 3 of Laming et al. (2014) for  $k_{\parallel}r_g$ , appropriate for the far upstream region of the cosmic ray precursor, and divided through by the cosmic ray gyroradius.

We identify  $\lambda_1/2 \sin \theta_1 = 5 \times 10^{17} \text{ cm}$  at a distance to Tycho of 3.2 kpc (Slane et al. 2014, model A), and taking  $\theta_1$  from Fig 3, we estimate  $\gamma_{max}$ . Letting  $\gamma_1 \rightarrow \gamma_{max}$ , and taking  $\eta = 0.26$ ,  $n_i = 0.3 \text{ cm}^{-3}$ , we find  $\gamma_{max} = 6 \times 10^5 - 1 \times 10^6$  corresponding to  $\theta_1 = 10^\circ - 15^\circ$ . Although model dependent, this broadly agrees with the modeling of Slane et al. (2014), who find the cosmic ray energy spectrum breaking from something close to a  $p^{-4}$  power law to a steeper fall-off just above  $\gamma \sim 10^5$  (their Fig. 4), and the original estimate of Eriksen et al. (2011), who simply identified the spacing of the stripes with a cosmic ray gyroradius. Projected onto the shock velocity vector, the wave phase varies with distance  $\lambda_1/2 \times \cos \theta_1 \simeq 1 \times 10^{17} - 1.5 \times 10^{17} \text{ cm}$ . Thus with a shock velocity of  $5000 \text{ km s}^{-1}$ , changes in the projected position of the stripes should be visible in  $2 \times 10^8 - 3 \times 10^8$

seconds, i.e. 6 - 10 years. Eriksen et al. (2011) report an intensity contrast of a factor of 25 between stripe maxima and minima. Relating this to  $B^{s+1}$  with  $s \sim 2.11$  we find a variation of  $B$  between maxima and minima of about a factor 3. This is significantly lower than the likely upstream magnetic field contrast of between a factor of 9 and 15, but probably reasonable when we consider that both polarizations are amplified upstream by this amount, and then the magnetosonic polarization is preferentially damped by transit time damping. In the case that the electron cooling time becomes longer than the Alfvén mode damping time, the variation of magnetic field along the shock front will be less clear, but stripes separated by  $\lambda_2/2$  oriented normal to  $\mathbf{k}_2$  extending further inside the shock would result, analogous to ripples associated with sound waves.

## 6. CONCLUSIONS

We suggest a model for the synchrotron “stripes” or ripples observed in Tycho’s SNR (Eriksen et al. 2011) based only on simple ideas about Alfvén propagation and

dissipation at the forward shock, calculated as a function of its obliquity. We find that the contrast is highest, and therefore that the stripes would be most visible for a narrow range of shock obliquities close to  $15^\circ$  in the case of strong Iroshnikov-Kraichnan turbulence. In our model, the emission comes from behind the shock front, once the magnetosonic component of the originally circularly polarized wave has been transit time damped. This is in contrast to previous ideas which have placed the structures giving rise to the synchrotron stripes in the shock precursor. In the model advanced here, some motion of the stripes over a period of one to a few years should be visible, leading to possibilities for an observational test.

This work was supported by Basic Research Funds of the Chief of Naval Research. I acknowledge enlightening conversations with Chee Ng, and I am grateful to Una Hwang and an anonymous referee for reading and commenting on the paper.

## APPENDIX

### MHD SHOCK RELATIONS

Here we reproduce a few relationships relating to MHD shock, following mainly Melrose (1986). The postshock perpendicular flow speed is

$$u_{2\perp} = u_1 \frac{(r-1) \sin \theta_1 \cos \theta_1}{M_{A1}^2 - r \cos^2 \theta_1} \rightarrow 0 \quad \text{as} \quad M_{A1} \rightarrow \infty. \quad (\text{A1})$$

The transverse magnetic field is

$$B_2 \sin \theta_2 = \frac{r(M_{A1}^2 - \cos^2 \theta_1)}{M_{A1}^2 - r \cos^2 \theta_1} B_1 \sin \theta_1 \rightarrow r B_1 \sin \theta_1 \quad \text{as} \quad M_{A1} \rightarrow \infty. \quad (\text{A2})$$

Writing

$$\frac{B_2 \sin \theta_2}{B_1 \sin \theta_1} = \frac{r(M_{A1}^2 - \cos^2 \theta_1)}{M_{A1}^2 - r \cos^2 \theta_1} = \frac{\cos \theta_1 \sin \theta_2}{\cos \theta_2 \sin \theta_1} \quad (\text{A3})$$

we find

$$\tan \theta_2 = r \tan \theta_1 + \frac{(r-1) \sin \theta_1 \cos \theta_1}{M_{A1}^2 - r \cos^2 \theta_1} = r \tan \theta_1 + \frac{1}{r} \tan \alpha \quad (\text{A4})$$

to be compared with

$$\cot \theta_{2W} = r \cot \theta_1 - \tan \alpha \quad (\text{A5})$$

from equation 6, for the wave refraction.

## REFERENCES

- Achterberg, A., & Blandford, R. D. 1986, MNRAS, 218, 551  
 Bamert, K., Kallenbach, R., Ness, N. F., et al. 2004, ApJ, 601, L99  
 Bell, A. R. 2004, MNRAS, 353, 550  
 Bell, A. R. 2005, MNRAS, 358, 181  
 Boldyrev, S. 2005, ApJ, 626, L37  
 Bykov, A. M., Osipov, S. M., & Ellison, D. C. 2011a, MNRAS, 410, 39  
 Bykov, A. M., Ellison, D. C., Osipov, S. M., Pavlov, G. G., & Uvarov, Y. A. 2011b, ApJ, 735, L40  
 Caprioli, D., & Spitkovsky, A. 2013, ApJ, 765, L20  
 Drury, L. O., & Falle, S. A. E. G. 1986, MNRAS, 223, 353  
 Eriksen, K., Hughes, J. P., Badenes, C., et al. 2011, ApJ, 728, L28  
 Gargaté, L., & Spitkovsky, A. 2012, ApJ, 744, 67  
 Goldreich, P., & Sridhar, S. 1995, ApJ, 438, 763  
 Hayato, A. et al. 2010, ApJ, 725, 894  
 Iroshnikov, P. 1963, Astron. Zh., 40, 742  
 Kraichnan, R. H. 1965, Phys. Fluids, 8, 1385  
 Laming, J. M., Hwang, U., Ghavamian, P., & Rakowski, C. E. 2014, ApJ, 790, 11  
 Laming, J. M., Moses, J. D., Ko, Y.-K., Murphy, R. J., Ng, C. K., Rakowski, C. E., & Tylka, A. J. 2013, ApJ, 770, 73  
 Malkov, M. A., Sagdeev, R. Z., & Diamond, P. H. 2012, ApJ, 748, L32  
 McKenzie, J. F., & Westphal, K. O. 1970, Phys. Fluids, 13, 630  
 Melrose, D. B. 1986, Instabilities in Space and Laboratory Plasmas (Cambridge: Cambridge University Press)  
 Rakowski, C. E., Laming, J. M., Hwang, U., Eriksen, K. A., Ghavamian, P., & Hughes, J. P. 2011, ApJ, 735, L21  
 Slane, P. O., Lee, S.-H., Ellison, D. C., Patnaude, D. J., Hughes, J. P., Eriksen, K. A., Castro, D., & Nagataki, S. 2014, ApJ, 783, 33  
 Vainio, R. & Schlickeiser, R. 1998, A&A, 331, 793  
 Vink, J., & Laming, J. M. 2003, ApJ, 584, 758  
 Vladimirov, A. E., Bykov, A. M., & Ellison, D. C. 2009, ApJ, 703, L29

- Webb, G. M., Zakharian, A., Brio, M., & Zank, G. P. 1999, J. Plasma Physics, 61, 295
- Zank, G. P., Li, G., Florinski, V., Hu, Q., Lario, D., & Smith, C. W. 2006, J. Geophys. Res. Space Phys., 111, 6108